Crystallization of calcium sulfate dihydrate in the presence of colloidal silica

Accepted for publication in *Industrial and Engineering Chemistry Research*
on September 27, 2010
Published article DOI: 10.1021/ie100309b

Fulin Wang, Thomas E. Davis, and Volodymyr V. Tarabara*

Department of Civil and Environmental Engineering, Michigan State University, East Lansing, MI 48824, USA.

Key Words:
gypsum, induction time, crystallization rate, crystal morphology, scaling, colloidal fouling

*Corresponding author. Phone: (517) 432-1755; Fax: (517) 355-0250; Email: tarabara@msu.edu

Abstract

The effects of silica colloids on calcium sulfate dihydrate (gypsum, $CaSO_4 \cdot 2H_2O$) crystallization are studied using feed solutions of varying degrees of supersaturation. A combination of light transmittance and electrical conductivity measurements is employed to characterize various aspects of the crystallization process. The induction time, nucleation rate, surface energy, and rate of crystallization of gypsum crystals are measured as functions of the saturation and the presence of non-crystallizing (SiO_2) colloids. Scanning electron microscopy (SEM) imaging is used to characterize the morphology of formed crystals. The induction time and the rate of crystallization are both shown to increase when gypsum crystal formed from solutions containing suspended colloids. The findings are rationalized in terms of a mechanistic model that links the random motion of colloids with nucleation and crystal growth processes. The results have important implications for a variety of industrially-relevant processes such as heat exchange and membrane separation and related fouling phenomena.

1. Introduction

In water treatment operations that use natural water as the source, fouling can be egregious. Membrane-based separation [1 2, 3] and heat transfer [4, 5] unit processes, for example, suffer significant efficiency losses due to fouling. The losses often translate into reduced quality and quantity of product water as well as increased energy consumption. Because the composition of most natural waters is complex, fouling by such waters is usually due to several concomitant processes, each corresponding to a distinct fouling mechanism. In heat exchangers, for example, scaling and particulate fouling are main mechanisms of fouling and typically occur simultaneously [6]. In reverse osmosis systems, formation of biofilm on the membranes surface (i.e., biological fouling) as well as fouling by precipitating salts and, in some cases, by colloids are of concern. While one fouling mechanism can dominate, there is growing evidence that interactions between different fouling mechanisms can be important [2, 4, 6, 7] and, in some cases, can govern the overall system performance [8].

Precipitative fouling by crystallizing sparingly soluble salts, also known as scaling, can severely impact performance of salt-rejecting membranes [9] and heat exchangers [4, 10]. Scaling is known to be influenced by other dissolved species such as surfactants [11], other aqueous ions [12,13, 14], and natural organic matter (NOM) [15]. The induced changes have been found to be specific to the interference agent. For example, in the presence of the cationic surfactant cetyltrimethylammonium bromide the induction time decreased and the growth efficiency of gypsum crystals increased; the anionic surfactant sodium

dodecyl sulfate had opposite effects [11]. The presence of another precipitating salt has been found to affect the structure and strength of gypsum scale in the manner that depended on the type of the salt [13]. Polyelectrolytes have also been shown to influence gypsum crystallization; the effect depended on the concentration, molecular weight, and composition of the polyelectrolyte [14]. Jiang et al. [16] have shown that the effect of borax (sodium borate, $Na_2B_4O_7$) on gypsum scaling depends on its concentration: gypsum scaling was expedited at low concentrations and retarded at high concentrations of borax. Studying gypsum crystallization during nanofiltration of agricultural drainage water, Le Gouellec and Elimelech [15] demonstrated that in the presence of NOM shorter gypsum crystals were formed.

Scaling is also known to be affected by suspended components of the natural water. Most of this knowledge comes from studies of heat exchangers, where the effect has been demonstrated to depend on the crystallizing ability of suspended particles [17, 18]. Having shown that crystallizing $CaCO_3$ particles greatly enhanced gypsum formation, Bansal et al. [4] attributed this effect to an increase in the number of nucleation sites. In the study on the deposition of colloids on heat exchanger plates, McGarvey and Turner [19] found that the rate of particle deposition was enhanced by $CaCO_3$ precipitation. The enhancing effect of crystallizing colloids was also reported by Andritsos and Karabelas [6], who demonstrated that $CaCO_3$ precipitation rate was greatly increased by fine aragonite ($CaCO_3$ polymorph) particles. In contrast, non-crystallizing particles were shown to either have no effect on scaling ($CaCO_3$ precipitation from solutions containing suspended silica [20], hematite [21] and silt [21]) or to reduce the amount of scale formed (gypsum precipitation from suspensions of alumina colloids [4]). Very little is known about the

influence of colloids on the crystallization of sparingly soluble salts in waters treated by salt-rejecting membranes. While both colloidal and precipitative fouling of membranes have been subjects of extensive research, there have been no studies published on the interaction between these two processes, which are often limiting the performance of nanofiltration and reverse osmosis membranes.

The objective of this work was to study how colloidal particles affect the kinetics of different stages of gypsum crystallization and the morphology of resultant crystals. The choice of silica as a representative non-crystallizing colloid was motivated by the abundance of colloidal SiO_2 in natural waters. Particles smaller then 100nm were selected as such smaller colloids are most likely to pass the pretreatment processes and impact the performance of salt-rejecting membranes used for softening and desalination. Gypsum was chosen as a salt of particular importance for membrane separations: while carbonate scaling can be prevented by decreasing the pH of the feed water, the precipitation of gypsum, which is insensitive to pH, is more difficult to control and remediate. The discussion of the observed effects of SiO_2 colloids on various aspects of gypsum crystallization is offered and the implications of the results are discussed.

2. Background

Crystallization in a supersaturated solution begins with nucleation that is the formation of nuclei that, once formed, may grow into larger crystals [22]. The degree of supersaturation is represented by the saturation, S_g. For gypsum, S_g is given by:

$$S_g = \frac{a_{Ca^{2+}} a_{SO_4^{2-}} a_w^2}{K_{sp}}, \quad (1)$$

where K_{sp} is the solubility product for $CaSO_4 \cdot 2H_2O$ in water (K_{sp} =2.623·10^{-5} at 20 ºC) [23]; a_i is the activity expressed as the product of the activity coefficient (γ_i) and the molality (m_i)of species i ($i = Ca^{2+}; SO_4^{2-}$; water). Davies' approximation can be used to estimate the activity coefficient as a function of ionic strength:

$$\log \gamma = -(Az^2 \frac{\sqrt{I}}{1+\sqrt{I}} - 0.3I), \quad (2)$$

where z is the ion charge; I is the ionic strength (M); A is 0.5 for aqueous solutions at (15 to 20) °C and 1 atm. The approximate range of applicability of eq. (2) is $I < 0.5$ M [24].

Induction time is defined as the time that elapses between the moment the supersaturation condition is achieved and the moment crystals are detected in the solution. Induction time

is known to be a function of the saturation, temperature and the presence of interferences [22, 25], and can be represented by a sum of three components [22, 26]:

$$t_{ind} = t_r + t_n + t_g , \tag{3}$$

where t_r is the relaxation time required for the system to achieve a quasi-steady-state distribution of molecular clusters; t_n is the time required for formation of stable nuclei, which grow into crystals instead of dissolving into the feed solution [27]; t_g is the time for the nucleus to grow to a detectable size. As the definition of t_g implies, the value of t_{ind} depends on the sensitivity of the technique used for detecting the crystals [25, 26]. Optical and electrochemical methods have been used to determine the induction time for gypsum. Optical methods include monitoring of scattered and transmitted light [27], measurement of turbidity [11, 28-30], and direct observation by the naked eye [31]. Electrochemical methods include measuring the conductivity of the feed suspensions [32] and measuring the concentration of free calcium cations in the solution [28, 33, 34]. The value of the induction time is specific to the measurement method and is usually defined operationally [25, 26].

For primary nucleation, the rate of nuclei formation (nucleation rate) is given by [26, 35]:

$$J_s = F \exp\left[\frac{-\beta \gamma_s^3 V_m^2 N_A f(\theta)}{(RT)^3 (\ln S_g)^2} \right], \tag{4}$$

where γ_s is the surface energy (interfacial tension) of the crystals (J/m^2); F is the pre-exponential factor (for homogeneous nucleation, F has a theoretical value of 10^{30} nuclei/(cm^3·s) [11]); T is the absolute temperature (K); β is the shape factor ($16\pi/3$ for spherical nuclei); V_m is the molecular volume for solid gypsum (m^3/mol); N_A is Avogadro's number (mol^{-1}); R is the gas constant (J/(mol·K)); $f(\theta)$ is a correction factor ($f(\theta)$ = 1 for homogenous nucleation and less than 1 for heterogeneous nucleation)

The surface energy (γ_s) can be calculated from the measured induction time using the following expression [26, 27, 29]:

$$\log t_{ind} = B + \frac{1}{T^3 (\log S_g)^2}\left[\frac{\beta \gamma_s^3 V_m^2 N_A f(\theta)}{(2.3R)^3}\right], \quad (5)$$

where B is a dimensionless constant.

The rate of gypsum crystallization is given by [36]:

$$\frac{dm}{dt} = k_b (C_b - C_s), \quad (6)$$

where m is the mass of gypsum formed; k_b is the gypsum bulk crystallization rate (also called the diffusion-controlled crystallization constant [36]); C_b is the gypsum

concentrations in bulk solution; C_s is the saturation concentration of gypsum. When the volume of the feed solution is constant, Eq. (6) may be rewritten as

$$\frac{dC}{dt} = k_b^{'}(C_b - C_s)\,, \tag{7}$$

where $k_b^{'}$ is the crystallization rate.

3. Material and methods

3.1. Experimental apparatus

The schematic of the batch reactor used in crystallization experiments is shown in Fig. 1. A 1,500 mL Pyrex® beaker with 1,000 mL of stirred feed solution was placed in a water bath, which was maintained at (20 ± 0.2) ºC using a programmable circulating chiller (model 9512, PolyScience, Niles, IL). The feed solution was mixed using magnetic stirring (3 inch stirrer bar) at a rate of 120 rpm and continuous circulation (gear pump EW-74013-20, Cole-Parmer, Vernon Hills, Illinois) at a flowrate of 1.6 L/min.

A small portion of the circulated solution was diverted into a flow-through UV-vis sample cell for on-line optical transmittance measurements in the (400 to 800) nm wavelength range (Multi-Spec 1501 spectrophotometer, Shimadzu, Kyoto, Japan). A decline of 5% in the light transmittance at 400 nm was used as the criterion to indicate the onset of gypsum crystallization [27]. Although optical transmittance was recorded in the (400 to 800) nm wavelength range, the transmittance at 400 nm was chosen for detection as we found the transmittance at lower wavelengths to be more sensitive to nucleation-caused changes in the optical properties of the feed (see Fig. S1, Supporting Documentation (SD)). The electrical conductivity was measured in real time using a conductivity probe (model 013005A, Thermo Electron Corp. Beverly, MA) and meter (model Orion 550, Thermo Electron Corp.) The electrical conductivity and optical

transmittance data were logged to a PC every 30 sec or 2 min, depending on the value of the initial saturation.

[Figure 1]

The experimental system described above was not designed to guarantee the homogeneous nucleation regime. Even when working with highly controlled precipitation reactors it is extremely difficult to ascertain the absence of impurities that provide an external surface and to completely exclude the possibility of heterogeneous nucleation. Instead, we have determined a posteriori which nucleation regime we had in our experiments based on the dependence of the induction time on saturation. We observed a linear dependence of $\ln(t_{ind})$ on $\ln^{-1}(S)$ dependence with an abrupt change in slope (see SD; Fig. S2); this change in slope can be attributed to the transition between the two regimes of nucleation (homogeneous and heterogeneous) that is followed by polynuclear growth [37]. For this induction scenario, homogeneous nucleation dominates at high saturations while at low saturations nucleation is heterogeneous. In our experiments heterogeneous nucleation occurred for saturations in the S = (1.5 to 2.3) range while homogeneous nucleation took place at higher saturations S = (2.3 to 3.24).

3.2. Regents, silica colloids, and feed suspensions

All reagents were of ACS analytical grade or higher (Fisher Scientific, Pittsburgh, PA) and were used without further purification. The ultrapure water used in the experiments

was supplied by a commercial ultrapure water system (Lab Five, USFilter Corp., Hazel Park, MI) equipped with a terminal 0.2 μm capsule microfilter (PolyCap, Whatman Plc., Sanford, ME). The resistance of water was greater than 16 $\mathrm{M\Omega \cdot cm}$. No buffers were added to the feed water.

Silica nanoparticles were obtained from the vendor as aqueous suspensions (SnowTex-XL and SnowTex-N, Nissan Chemical America Corp., Houston, TX). Light scattering data (ZetaPALS, Brookhaven Instrument Corp., Holtsville, NY) showed that SiO_2 particle size distribution was relatively narrow (polydispersity factor of 0.074) with a mean hydrodynamic particle diameter of (56 ± 1) nm for SnowTex-XL and (16 ± 0) nm for SnowTex-N suspensions. The pH of the 50 mg/L aqueous suspension of the SnowTex-XL colloids was measured to be 7.5.

The feed solutions supersaturated with respect to gypsum were prepared by dissolving two highly soluble salts - $CaCl_2 \cdot 2H_2O$ and Na_2SO_4 - separately, one after another. The amount of $CaCl_2 \cdot 2H_2O$ and Na_2SO_4 added and the resulting degree of supersaturation are shown in Table 1. Note that ionic strengths were within the approximate range of applicability of the Davies' equation ($I < 0.5\,\mathrm{M}$).

[Table 1]

3.3. Characterization of the gypsum crystals

To comparatively characterize gypsum crystals formed in experiments with feed waters of different compositions, 10 mL samples of the feed were withdrawn from the batch reactor at the point in the experiment when the optical transmittance of the feed decreased to 50% of its initial value. The samples were withdrawn using a syringe and were filtered through a polycarbonate track-etch membrane (Nuclepore®, Whatman Plc.) with a 0.1 μm nominal pore size. Immediately after the filtration, 5 mL of methanol were filtered through the membrane to remove the residual feed solution so that no additional gypsum could crystallize on surface of crystals deposited on the membrane during filtration. The membrane filter was then dried in air at room temperature.

For SEM imaging, a small (approximately1 cm^2) coupon of the dried membrane was cut out and coated with osmium for 30 s (Neoc-AN coater, Meiwa Shoji Co. Ltd., Kyoto, Japan). SEM micrographs were recorded using Hitachi S-4700II Field Emission scanning electron microscope (Hitachi High Technologies America, Inc. Pleasanton, CA). The microscope was operated in the ultra-high resolution mode with an accelerating voltage of 15 kV and an emission current of 10 μA.

4. Results and discussion

The assumption of homogenous nucleation was only valid for the S = (2.3 to 3.24) range of saturation (Fig S2; SD). Therefore, the values of surface energy, nucleation rate and crystallization rate are reported for this range of saturations.

4.1. Effect of silica colloids on gypsum induction time

First, in a control crystallization experiment, the optical transmittance and the electrical conductivity of the SiO_2-free oversaturated feed solution were recorded as functions of time. Transmittance and conductivity decreased to 95% of their initial values after 22.8 min and 38 min, respectively, indicating that optical transmittance is a more sensitive indicator of the presence of nucleated gypsum crystals in the feed (Fig. 2).

[Figure 2]

The evolution of optical transmittance and electrical conductivity of feed solutions with different initial saturation indices is shown in Fig. 3. Based on the optical transmittance data, values of t_{ind} were determined (Fig. 4a). The introduction of SiO_2 colloids to the feed resulted in an increase in the induction time for gypsum. This effect was more evident for feed solutions with lower initial saturation indices (see SD, Fig. S3).

[Figure 3]

4.2. Effect of silica colloids on the surface energy and nucleation rate of gypsum crystals

From the slope of the $\log(t_{ind})$ versus $1/(\log S_g)^2$ plot (Eq. (5)), the value of surface energy, γ_s, was calculated to be 7.94 ± 0.21 J/m^2 for gypsum crystals formed from SiO_2–free solutions and 7.95 ± 0.06 J/m^2 for gypsum crystals formed from solutions with 50 mg/L loading of colloidal SiO_2. The standard deviations given above correspond to the 90% confidence interval. Thus, within the experimental error of our measurements, the presence of silica colloids did not have an effect on the surface energy of crystals.

[Figure 4]

Based on Eq. (4), the theoretical nucleation rates of gypsum crystallization at different saturation indices were calculated. The presence of silica colloids was found to have no evident effect on the nucleation rate (Fig. 4b).

4.3. Effect of silica colloids on gypsum crystallization rate

Because the absorption and scattering of light by a suspension depends on both the number and the size of suspended particles (i.e., gypsum nuclei and crystals in our case) [38], optical transmittance could not be used as a quantitative measure of the amount of gypsum crystal formed. The crystallization rate can be directly measured, however, by determining how fast free Ca^{2+} and SO_4^{2-} ions disappear from the solution as they become

incorporated into the growing $CaSO_4$ crystals. Based on the fact that free Ca^{2+} and SO_4^{2-} contribute to conductivity while $CaSO_4$ crystals do not, we used the measured conductivity decline with time $t > t_{ind}$ to determine dC/dt (Eq. (7)) for feed solutions with different initial saturation indices in the absence and in the presence of SiO_2 colloids (Fig. 4c). For all saturation conditions, the introduction of silica colloids led to a higher gypsum crystallization rate. The increase was larger for feed solutions with higher initial saturation indices.

Hypothetical mechanistic description of the observed effects of SiO_2 colloids

We hypothesize that the delayed induction of gypsum crystals in the presence of colloidal particles is a result of collisions between the colloids and nascent $CaSO_4$ nuclei. The nuclei have to grow into a critical size to become stable sites available for further growth, the process that can be disrupted by collisions with SiO_2 nanoparticles undergoing Brownian diffusion. The kinetic energy of the Brownian motion of colloids ($1.5k_BT$) is smaller than but is of the same order of magnitude as the activation energy for gypsum crystallization (30 kJ/mol [39], which is equivalent to $3.65k_BT$ at T=20^0C).

The same random diffusion of colloids can lead to enhanced local mixing in the vicinity of already stable and growing $CaSO_4$ crystals. Large “fluidized particles” have been successfully applied to improve mass transfer in membrane modules (e.g., [40]) In experiments with SnowTex-XL colloids, we showed that introducing the colloids into the feed of reverse osmosis membranes results in improved mass transfer; this improvement

manifested itself as an increase in salt rejection by the membranes, which was attributed to the local mixing of the salt concentration polarization layer by the silica colloids [41]. Such mixing should mitigate the diffusional limitation on the transport of Ca^{2+} and SO_4^{2-} to the growth sites on the $CaSO_4$ crystal surface. In consistence with this hypothesis, longer induction times were recorded in experiments on gypsum crystallization in the presence of 16 nm colloids than in experiments with 56 nm colloids (Figure 5). The smaller colloids have higher diffusion coefficient and, therefore should provide better mixing. Although largely speculative, this mechanistic model explains both the delay in the induction and faster rates of crystallization from colloid-bearing solutions.

4.4. Effect of silica colloids on the morphology of gypsum crystals

SEM imaging demonstrated that gypsum crystals formed in the absence of SiO_2 colloids were predominantly needle-like with a typical length-to-width ratio of approximately 20 (Fig. 6). There was no evidence of the epitaxial $SiO_2/CaSO_4 \cdot 2H_2O$ growth. Interestingly, there was a significant number of rosette-shaped crystals; these likely represented the needle-like crystals in an early stage of growth. In contrast, when the SiO_2 colloids were present, gypsum crystals with predominantly plate-like morphology with a typical length-to-width ratio of approximately 2 were formed. SEM imaging showed the presence of silica colloids deposited on the surface of gypsum crystals (as seen in Figures 6f, 6h). Given that no colloids were observed to be incorporated inside gypsum crystals (i.e., no epitaxial growth), we believe the colloids were deposited onto the crystal surface during drying at the time of SEM sample preparation. There were also some needle-like crystals with the length-to-width ratio varying significantly from one crystal to another. The surface of these crystals was rougher than that of crystals formed in the absence of SiO_2 colloids. No rosette-shaped crystals were observed.

[Figure 5]

In earlier studies, similar changes in the morphology of gypsum crystals formed in the presence of additives were reported. For example, the addition of cetyltrimethylamonium bromide to a solution supersaturated with respect to gypsum decreased the length-to-width ratio of gypsum crystals that were formed [11]; in another study, the presence of 0.1

g/L nitrilotrimethylenephosphonic acid resulted in the formation of much larger plate-shaped crystals [42]. In both of these cases, an increase in the surface energy was reported to accompany the morphological changes. In contrast with this study, we did not observe a statistically significant change in the surface energy of gypsum crystals although their morphology has changed markedly.

4.5. Implications for industrial processes

The observed colloid-induced changes in the morphology of gypsum crystals may be important in gypsum precipitation processes that include a solid-liquid separation step such as removal of by-product gypsum in phosphoric acid manufacturing process [11, 43]. The reported effects of colloids may also be significant in processes involving the conversion of calcium sulfate dihydrate into calcium sulfate hemihydrate wherein the large size and the plate-like morphology of gypsum crystals are preferred [44]. These findings can be useful in understanding the effect of smaller colloids capable of passing the pretreatment stage on the performance of salt rejecting membranes used in water softening or desalination. The results presented in this work indicate that under conditions of concomitant fouling of membranes by scale and colloids, the characteristics of the precipitation of poorly soluble salts such as gypsum will be altered by the presence of colloidal particles; such changes are very likely to be important in determining the overall efficiency of membrane separation. Finally, from the process design perspective, the demonstrated effect of non-crystallizing colloids on the crystallization process points to the possibility of controlling the size and morphology of crystals using particulate additives.

5. Conclusions

The effect of silica colloids on gypsum scaling was studied in a series of batch experiments with feed solutions of varying degrees of supersaturation. The induction time of gypsum crystallization and gypsum crystallization rate were found to increase, while the nucleation rate and the surface energy of the crystals remained unaffected when SiO_2 colloids were present in the feed. Larger, plate-like crystals were formed from solution with suspended SiO_2. This was in sharp contrast to the needle-like morphology typical for gypsum crystals formed from colloid-free solutions. The results have implications for a variety of industrially-relevant processes including heat exchange and membrane separation. In particular, the results can be useful in understanding the effect of small colloids capable of passing the pretreatment stage on the performance of heat exchangers and salt rejecting membranes used in water softening or desalination.

Acknowledgments

This work was supported by the National Water Research Institute (project no. 05-TM-007) and the National Science Foundation (research grant OISE-0530174). We thank Pall Corp. for providing the UF membrane samples and Nissan Chemical America Corp. for supplying the silica suspension. We also thank Dr. Ewa Danielewicz from the Center for Advanced Microscopy at Michigan State University for her assistance with SEM sample preparation.

Nomenclature

A	dimensionless coefficient
B	dimensionless constant
C	gypsum concentration (mol/L)
C_b	gypsum concentration in bulk solution (mol/L)
C_s	saturation concentration of gypsum (mol/L)
F	frequency constant
$f(\theta)$	correction factor
I	ionic strength (M)
J_s	nucleation rate (nucleus/(m^3·s))
k_b	gypsum bulk crystallization rate (g·L/(min·mol))
$k_b^{'}$	gypsum crystallization rate (min^{-1})
K_{sp}	solubility product
m	mass of gypsum crystals (g)
N_A	Avogadro's number (mol^{-1})
R	gas constant (J/(mol·K))
S_g	saturation
T	absolute temperature (K)
t_{ind}	induction time (min)
V_m	molecular volume (m^3/mol)
z	ion charge

Greek letters

α	fraction of calcium and sulfate ions existing as ion pairs
β	shape factor
γ	activity coefficient
γ_s	surface energy of the crystals (J/m^2)
ρ^2	correlation coefficient

References

1. Committee Report: Recent advances and research needs in membrane fouling. *J. Am. Water Works Assoc.* **2005,** 97, (8), 79-89.
2. Trussell, R. S.; Merlo, R. P.; Hermanowicz, S. W.; Jenkins, D., The effect of organic loading on process performance and membrane fouling in a submerged membrane bioreactor treating municipal wastewater. *Wat. Res.* **2006,** 40, (14), 2675.
3. Rosenberger, S.; Laabs, C.; Lesjean, B.; Gnirss, R.; Amy, G.; Jekel, M.; Schrotter, J. C., Impact of colloidal and soluble organic material on membrane performance in membrane bioreactors for municipal wastewater treatment. *Wat. Res.* **2006,** 40, (4), 710.
4. Bansal, B.; Muller-Steinhagen, H.; Chen, X. D., Effect of suspended particles on crystallization fouling in plate heat exchangers. *J. Heat Transfer, Trans. ASME* **1997,** 119, (3), 568.
5. Grandgeorge, S.; Jallut, C.; Thonon, B., Particulate fouling of corrugated plate heat exchangers. Global kinetic and equilibrium studies. *Chem. Eng. Sci.* **1998,** 53, (17), 3050.
6. Andritsos, N.; Karabelas, A. J., The Influence of particulates on CaCO3 scale formation. *J. Heat Transfer* **1999,** 121, 225-227.
7. Lee, S.; Cho, J.; Elimelech, M., Combined influence of natural organic matter (NOM) and colloidal particles on nanofiltration membrane fouling. *J. Membr. Sci.* **2005,** 262, 27-41.
8. Wang, F.; Tarabara, V. V. In *Coupled effects of scaling and colloidal deposition on the performance of reverse osmosis membranes*, The 233rd ACS National Meeting, Chicago, IL, March 2007; Chicago, IL, March 2007.
9. Uchymiak, M.; Rahardianto, A.; Lyster, E.; Glater, J.; Cohen, Y., A novel RO ex situ scale observation detector (EXSOD) for mineral scale characterization and early detection. *J. Membr. Sci.* **2007,** 291, (1-2), 86.
10. Karabelas, A., Scale formation in tubular heat exchangers--research priorities. *International Journal of Thermal Sciences* **2002,** 41, (7), 682.
11. Mahmoud, M. H. H.; Rashad, M. M.; Ibrahim, I. A.; Abdel-Aal, E. A., Crystal modification of calcium sulfate dihydrate in the presence of some surface-active agents. *J. Colloid Interface Sci.* **2004,** 270, (1), 99-105.
12. He, S. L.; Oddo, J. E.; Tomson, M. B., The Inhibition of Gypsum and Barite Nucleation in Nacl Brines at Temperatures from 25-Degrees-C to 90-Degrees-C. *Applied Geochemistry* **1994,** 9, (5), 561-567.
13. Sheikholeslami, R., Mixed salts -- scaling limits and propensity. *Desalination* **2003,** 154, (2), 117.
14. Amjad, Z.; Hooley, J., Influence of polyelectrolytes on the crystal growth of calcium sulfate dihydrate. *J. Colloid Interface Sci.* **1986,** 111, (2), 496.
15. Le Gouellec, Y. A.; Elimelech, M., Calcium sulfate (gypsum) scaling in nanofiltration of agricultural drainage water. *J. Membr. Sci.* **2002,** 205, (1-2), 279.
16. Jiang, W.; Pan, H.; Tao, J.; Xu, X.; Tang, R., Dual roles of borax in kinetics of calcium sulfate dihydrate formation. *Langmuir* **2007,** 23, 5070-5076.
17. Sheikholeslami, R., Composite fouling of heat transfer equipment in aqueous media - a review. *Heat Transfer Engineering* **2000,** 21, (3), 34 - 42.

18. Hasson, D. In *Progress in precipitation fouling: a review, in:Understanding Heat Exchanger Fouling and its Mitigation, T.R. Bott et al. (Eds)*, 1999; Begell House, New York: 1999; pp 67-89.
19. McGarvey, G. B.; Turner, C. W., Synergism models for heat exchanger fouling mitigation. In: T.R. Bott et al.Understanding Heat Exchanger Fouling and its Mitigation, Begell House, New York **1999**, 155-161.
20. Okazaki, M.; Kimura, S., Scale formation on reverse-osmosis membranes *J. Chem. Eng. Jpn.* **1984,** 17, (2), 145.
21. Hasson, D.; Drak, A.; Semiat, R., Inception of CaSO4 scaling on RO membranes at various water recovery levels. *Desalination* **2001,** 139, (1-3), 73-81.
22. Mullin, J. W., *Crystallization*. 4th ed.; Butterworth-Heinemann: Oxford, 2001.
23. Nordstrom, D. K.; Plummer, L. N.; Langmuir, D.; Busenberg, E.; May, H. M.; Jones, B. F.; Parkhurst, D. L., Revised chemical equilibrium data for major water-mineral reactions and their limitations, in Bassett, R.L. and Melchior, D. eds., Chemical modeling in aqueous systems II: Washington D.C., American Chemical Society Symposium Series 416, Chapt. 31. **1990**, 398-413.
24. Appelo, C. A. J.; Postma, D., *Geochemistry and groundwater pollution*. Balkema: Rotterdam, 2005.
25. Söhnel, O.; Mullin, J. W., A method for the determination of precipitation induction periods. *J. Crystal Growth* **1978,** 44, 377 - 382.
26. Söhnel, O.; Mullin, J. W., Interpretation of crystallization induction periods. *J. Colloid Interface Sci.* **1988,** 123, (1), 43-50.
27. Lancia, A.; Musmarra, D.; Prisciandaro, M., Measuring induction period for calcium sulfate dihydrate precipitation. *AIChE J.* **1999,** 45, (2), 390 - 397.
28. Shih, W. Y.; Albrecht, K.; Glater, J.; Cohen, Y., A dual-probe approach for evaluation of gypsum crystallization in response to antiscalant treatment. *Desalination* **2004,** 169, (3), 213.
29. He, S.; Oddo, J. E.; Tomson, M. B., The inhibition of gypsum and barite nucleation in NaCl brines at temperatures from 25 to 90[degree sign]C. *Appl. Geochem.* **1994,** 9, (5), 561.
30. Hasson, D.; Drak, A.; Semiat, R., Inception of $CaSO_4$ scaling on RO membranes at various water recovery levels. *Desalination* **2001,** 139, 73 - 81.
31. Lam, W. H.; Ng, K. M., Diastereomeric salt crystallization synthesis for chiral resolution of ibuprofen. *AIChE J.* **2007,** 53, (2), 429 - 437.
32. Klepetsanis, P. G.; Koutsoukos, P. G., Kinetics of calcium sulfate formation in aqueous media: effect of organophosphorous compounds. *J. Crystal Growth* **1998,** 193, 156 - 163.
33. Le Gouellec, Y. A.; M., E., Control of calcium sulfate (gypsum) scale in nanofiltration of saline agricultural drainage water. *Environ. Eng. Sci.* **2002**, (19), 387-397.
34. Hina, A.; Nancollas, G. H.; Grynpas, M., Surface induced constant composition crystal growth kinetics studies. The brushite–Gypsum system. *J. Crystal Growth* **2001,** 223, (1-2), 213 - 224.
35. Myerson, A. S., *Handbook of Industrial Crystallization*. 2nd ed.; Butterworth-heinemann: Boston, 2002; p 33-63.
36. Nancollas, G. H., The growth of crystals in solution. *Adv. Colloid Interface Sci.* **1979,** 10, 215-252.

37. Sohnel, O.; Mullin, J. W., Interpretation of Crystallization Induction Periods. *Journal of Colloid and Interface Science* **1988,** 123, (1), 43-50.
38. Naganuma, T.; Kagawa, Y., Effect of particle size on light transmittance of glass particle dispersed epoxy matrix optical composites. *Acta Mater.* **1999,** 47, (17), 4321 - 4327.
39. Liu, S. T.; Nancollas, G. H., Kinetic and morphological study of seeded growth of calcium-sulfate dihydrate in presence of additives. *J. Colloid and Interface Sci.* **1975,** 52, (3), 593-601.
40. van der Waal, M. J.; van der Velden, P. M.; Koning, J.; Smolders, C. A.; van Swaay, W. P. M., Use of fluidized beds as turbulence promoters in tubular membrane systems,. *Desalination* **1977,** 22, 465-483.
41. Wang, F. L.; Tarabara, V. V., Coupled effects of colloidal deposition and salt concentration polarization on reverse osmosis membrane performance. *J. Membr. Sci.* **2007,** 293, (1-2), 111-123.
42. Prisciandaro, M.; Olivieri, E.; Lancia, A.; Musmarra, D., Gypsum precipitation from an aqueous solution in the presence of nitrilotrimethylenephosphonic acid *Ind. Eng. Chem. Res.* **2006,** 45, 2070 - 2076.
43. Rashad, M. M.; Baioumy, H. M.; Abdel-Aal, E. A., Structural and spectral studies on gypsum crystals under simulated conditions of phosphoric acid production with and without organic and inorganic additives. *Cryst. Res. Technol.* **2003,** 38, (6), 433 - 439.
44. Kojima, Y.; Yasue, T., Synthesis of large plate-like gypsum dihydrate from waste gypsum board. *J. Euro. Ceram. Soc.* **2006,** 26, (4-5), 777-783.

List of Figures

List of Tables

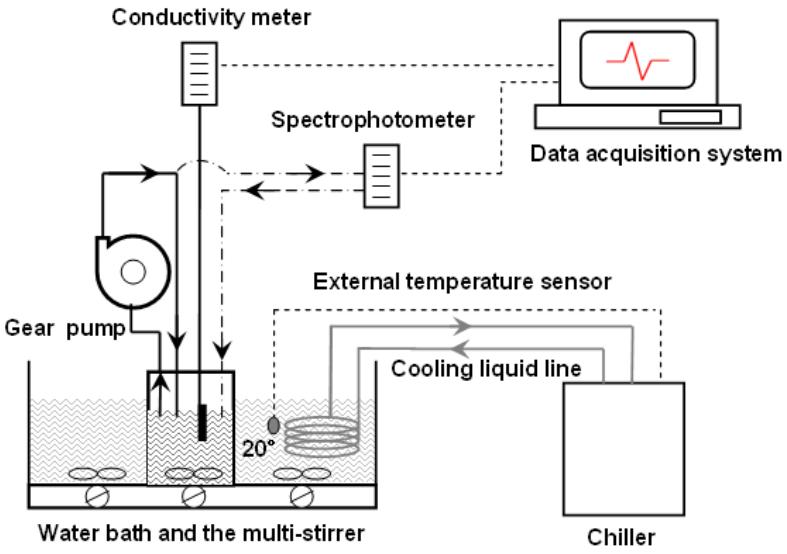

Figure 1: Schematic of the batch reactor used in crystallization experiments.

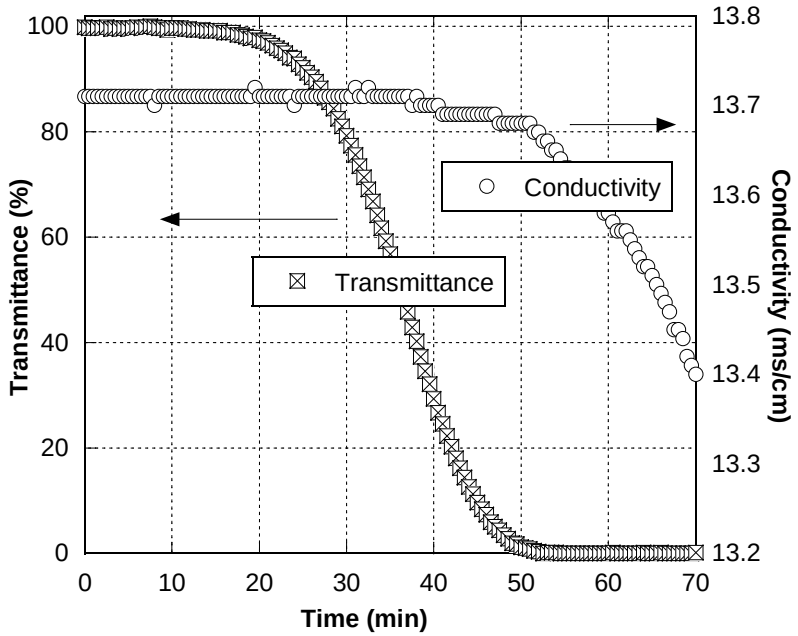

Figure 2: Transmittance and conductivity measurement for determining the induction time (measurements were for the feed solution in the batch);(S_g = 2.75; no silica colloids).

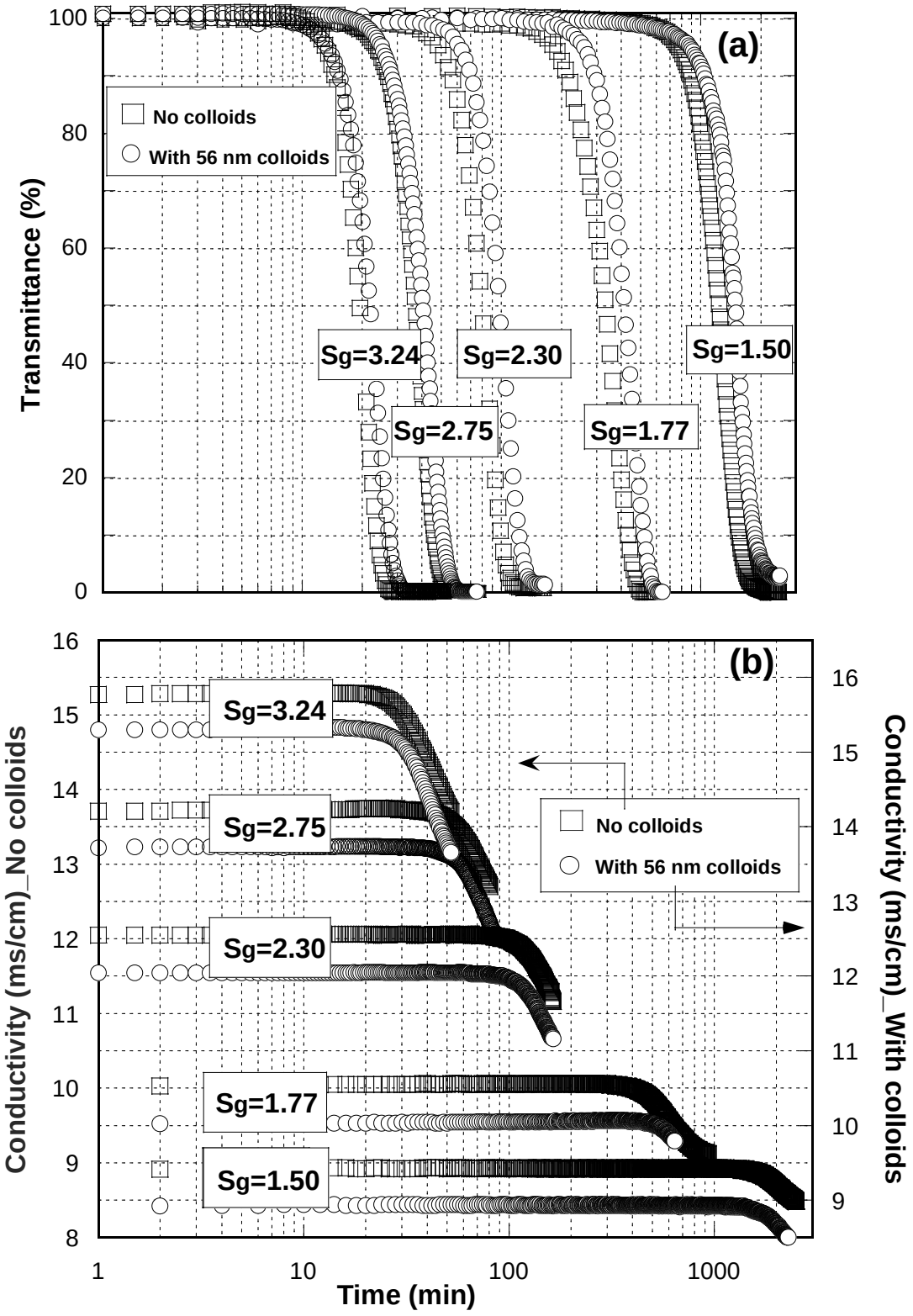

Figure 3: Effect of silica colloids on changes in the optical transmittance (a) and electrical conductivity (b) with time for feed solutions at five different values of saturation.

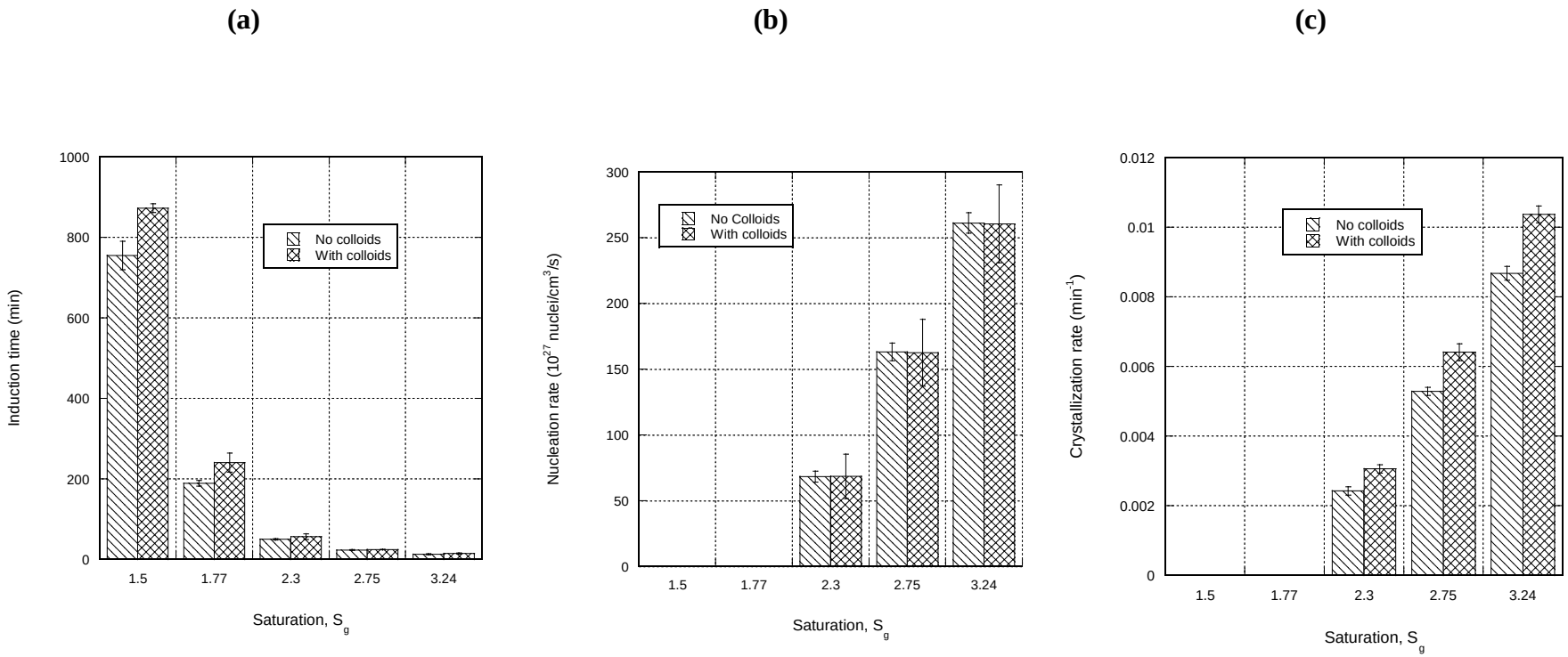

Figure 4: Effect of 56 nm silica colloids on (a) induction time, (b) nucleation rate, and (c) crystallization rate of gypsum. Nucleation and crystallization rates are not reported for lower saturations that correspond to heterogeneous nucleation regime. Error bars on Fig 4(b) denote the range of nucleation rates that corresponds to the 95% confidence interval for the value of the surface energy, γ_s.

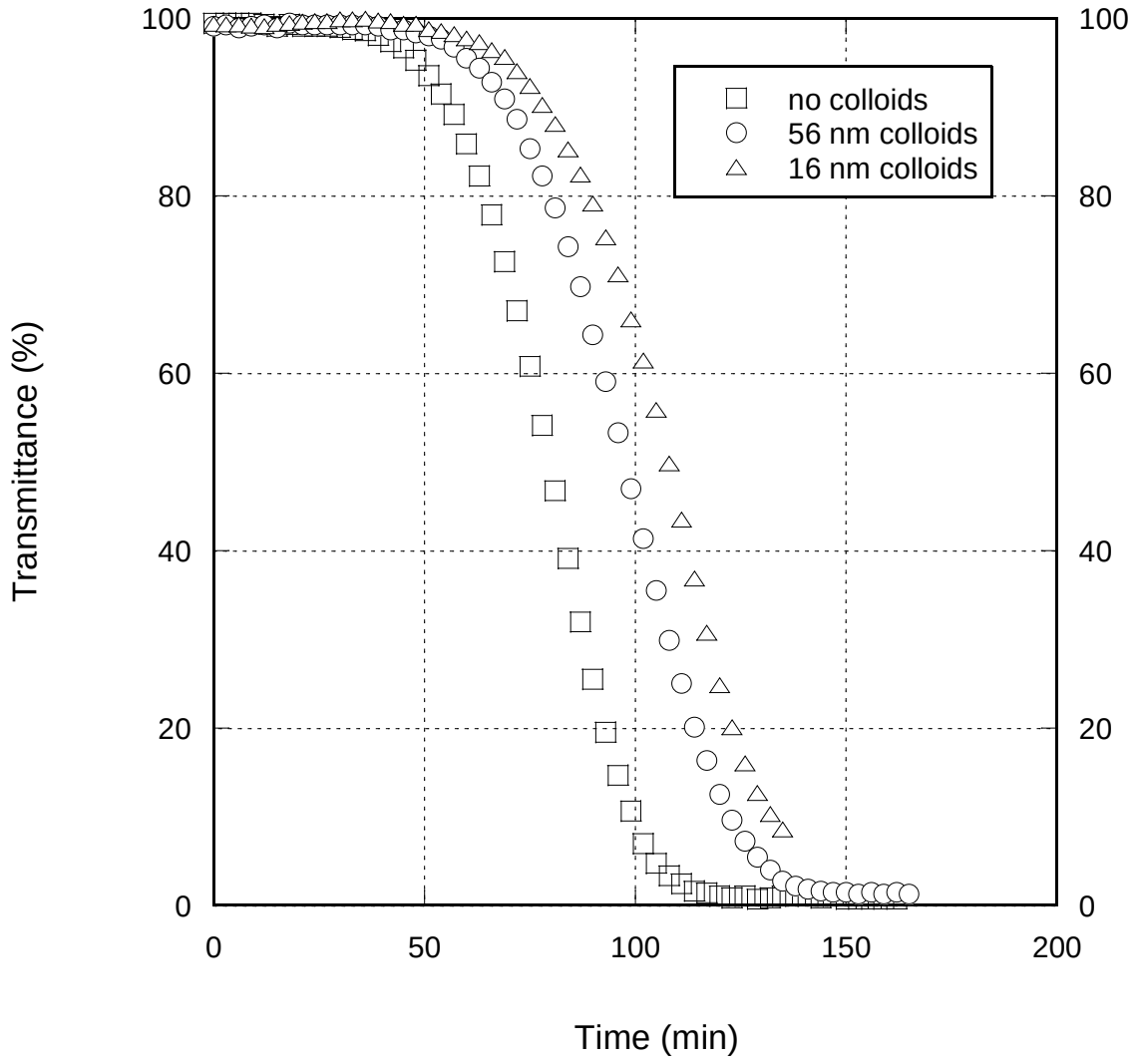

Figure 5: Effect of silica colloids of two different sizes on changes in the optical transmittance with time for feed solutions at the saturation S_g =2.30. The induction times were determined to be (70.3 ± 5.0) min and (56.3 ± 7.1) min in experiments with 16 nm colloids and 56 nm SiO_2 colloids, correspondingly.

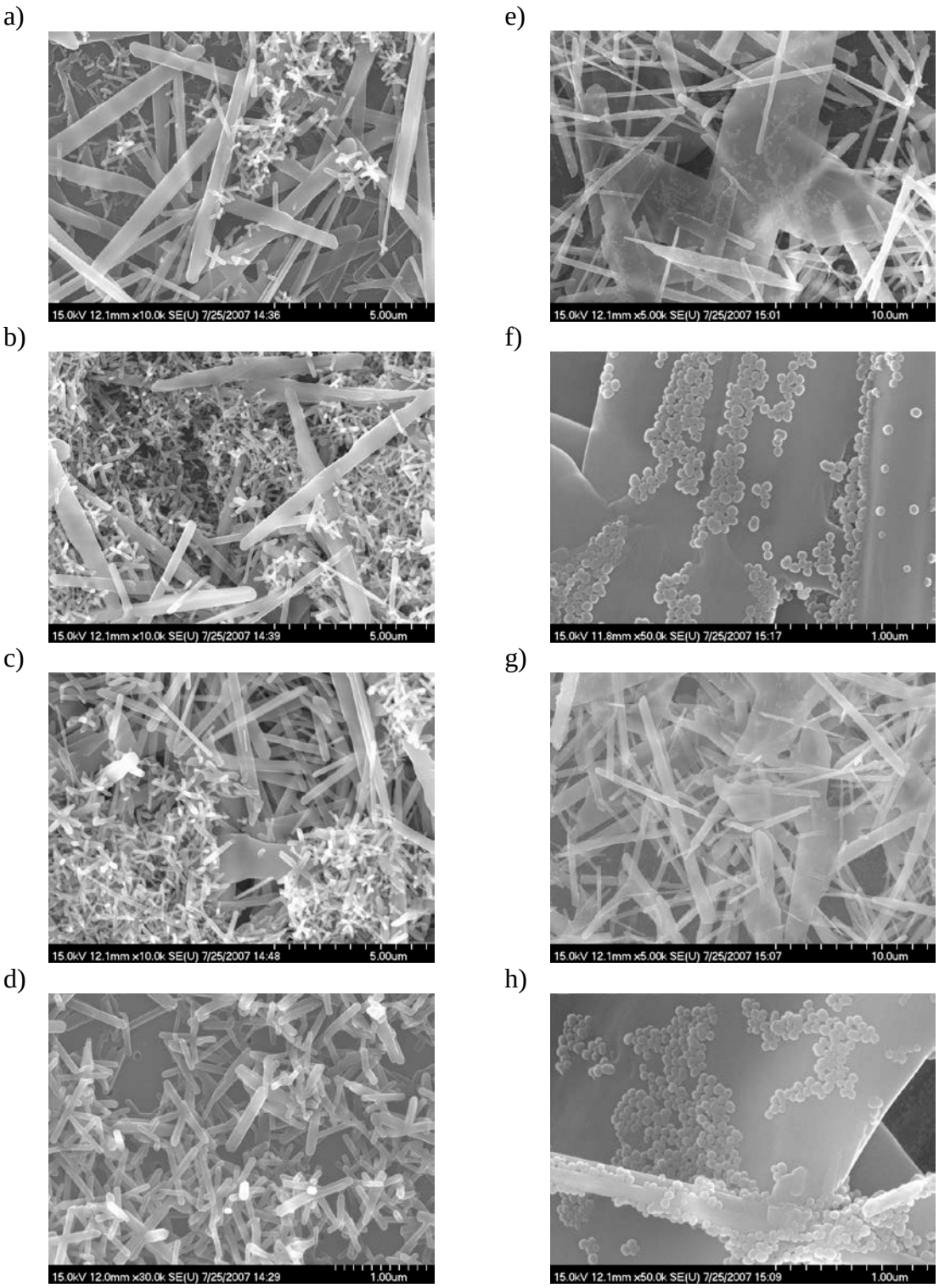

Figure 6: SEM images of gypsum crystals formed in the absence (a-d) and in the presence (e-h) of 50 mg/L silica colloids. Conditions: S_g = 2.75, transmittance = 50%.

The two groups of images were chosen to represent the variety of crystal morphologies observed under the two sets of conditions (i.e., presence or absence

of colloidal silica).

$CaCl_2 2H_2O$	Na_2SO_4	S_g *	α #	I #	S_g #
g/L	g/L		%	mM	
3.80	3.67	2.83	30.0	118.6	1.50
4.35	4.21	3.40	30.8	134.4	1.77
5.38	5.20	4.53	32.1	163.0	2.30
6.24	6.02	5.52	33.1	186.2	2.75
7.09	6.85	6.58	34.0	208.9	3.24

Table 1: Composition of model solutions.

* Computed without taking ion formation into account
# Computed using Visual Minteq with the formation of ion pairs taken into account